NUMERICAL INVESTIGATION OF NATURAL GAS FEASIBILITY IN A DIRECT INJECTION HEAVY-DUTY DIESEL ENGINE

Riad HADJAB [a*] ***and Mahfoud KADJA*** [b]

[a]University of Kasdi Merbah Ouargla, Algeria

[b]Laboratory of Applied Energetics and Pollution, Department of Mechanical Engineering, University of Mentouri, Constantine, Algeria

* Corresponding author: hadjab_riad@hotmail.com

In the present study, numerical simulations were performed on a direct injection heavy-duty diesel engine. Methane, which is the predominant component in natural gas, was chosen as the fuel. The simulations involved five exhaust gas recirculation ratios (0%, 10%, 20%, 25%, and 30%) to examine their effect on engine performance, NOx, and soot emissions. The numerical results were compared with existing experimental measurements of a typical diesel engine without exhaust gas recirculation. A comparison of the numerical results of the four cases of exhaust gas recirculation ratios reveals that the 30% exhaust gas recirculation ratio achieves a significant reduction in NOx emissions without increasing soot emissions. Consequently, the engine meets the authorized emission standards without excessive performance degradation.

Keywords: natural gas, diesel engine, NOx, soot, exhaust gas recirculation, fluent CFD

1. Introduction

Natural gas is a promising alternative fuel for internal combustion engines because of its low emission potential, reasonable cost, and domestic availability. To match the performance and efficiency of conventional diesel engines, the heavy-duty engine industry has adopted the technology of using natural gas in compression ignition engines. This technology is known as direct injection natural gas (DING) engines. In theory, it is possible to burn natural gas as a single fuel using a compression ignition engine. However, because of its high auto-ignition temperature, natural gas does not spontaneously ignite at the required time when injected into the combustion chamber of a typical diesel engine. To overcome this challenge, a system for high-pressure direct injection of natural gas and pilot diesel fuel was developed, where a small diesel pilot is injected first and ignites spontaneously from compression, followed shortly by natural gas injection, which is ignited by the diesel pilot's diffusion flame [1,2]. In the long term, the most promising technology for heavy-duty engines is direct injection using natural gas as a single fuel, initiated using other separate ignition sources such as a spark plug or glow plug [3,4]. This approach eliminates the need for a pilot diesel fuel and simplifies the combustion process, resulting in even lower emissions. The use of spark plug ignition assist has been suggested but was not considered suitable for such applications because of concerns over component durability [4]. Hot surface ignition assist is a recommended system for DING engines because it allows for the local increase of temperature in the combustion chamber

without the need for a complex two-fuel injector and two-fuel supply systems. From an environmental aspect, the advantage of using natural gas alone in a DING engine is that it generates less particulate matter than pilot diesel fuel. However, it is worth noting that both the DING engine and the pilot-injection natural gas engine generate NOx in similar proportions. Hence, employing an aggressive exhaust gas recirculation (EGR) system for reducing NOx in the DING engine is more feasible than in the pilot-injection natural gas engine, ensuring a satisfactory trade-off between particulate matter and NOx emissions [5]. Several numerical studies on DING engines have been presented in the literature, such as those by K. Pan, J. Wallace (2021), G. Papageorgakis (1996), P. Ouellette (1998), and W. H. Kurniawan (2008). However, to the best of our knowledge, pollutant emissions, especially NOx and soot, have rarely been studied numerically. The objective of this study is to investigate the combustion and emissions performance of a direct injection of natural gas into a diesel engine. This study focuses on the effects of EGR on in-cylinder effective pressure, NOx, and soot emissions. Pure methane was used in this study because it represents the largest fraction (often 90% or more) of natural gas. In addition, the detailed chemical reactions involved in the simulations are simpler than those in higher-order hydrocarbon fuels.

2. Problem description

Tab. 1 and Tab. 2 show the specifications and operating conditions for the engine, which have been previously employed in research related to combustion and pollutant emissions [6]. For this study, the amount of methane injected into the DING engine is set to 0.0666 g/cycle, whereas the typical amount of diesel fuel injected was set to 0.1622 g/cycle. This adjustment was made to approximately match the equivalent effective pressure (without EGR) of the diesel-fueled engine based on experimental results [6], as shown in Fig. 1. The simulated simplified representation of fuel mass flow profile is presented in Fig. 2. Fluent CFD software is used in this study to simulate the non-premixed combustion process of a four-stroke diesel engine [7], with methane as the fuel injected through the injector hole, as shown in Fig. 3. The simulation involves introducing the main species of the EGR into the oxidant flow, with different EGR ratios (10%, 20%, 25%, and 30%) applied to examine their effect on engine performance, NOx, and soot emissions.

Table 1. Engine specifications

Engine	Caterpillar 3401
Cylinder bore x stroke (mm)	137.19 x 165.1
Compression Ratio	15:1
Connected rod length (mm)	261.62
Combustion chamber geometry	Mexican Hat
Engine speed (RPM)	1600
Intake valve closing (IVC)	- 147 (ATDC)
Exhaust valve opening (EVO)	+136 (ATDC)

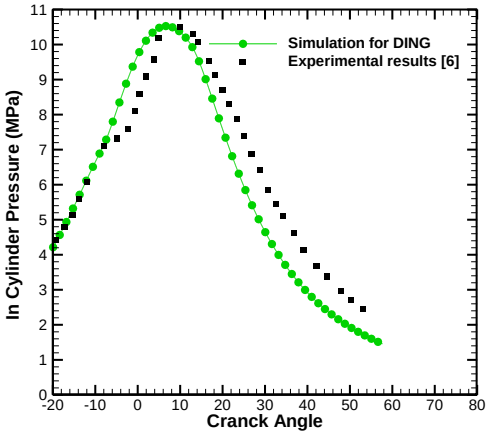

Figure 1. In-cylinder pressure for DING and a typical diesel engine

Table 2. Fuel injection

Number of nozzle holes	6
Nozzle hole diameter (mm)	0.259
Fuel injected (g/cycle)	0.1622
Start of injection (CA BTDC)	9°
Maximum Injection pressure (MPa)	90
Injection duration (CA)	21.5

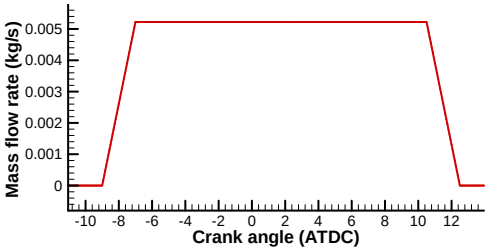

Figure 2. Simplified representation of fuel mass flow profile.

3. Computational domain and initial conditions

Fig. 4 illustrates the geometry and calculation field of the simplified engine model. The problem considers a 60-degree periodic slice of the piston–cylinder combination, which corresponds to one fuel nozzle hole. The simulation begins at the IVC position and ends at the EVO position, with no valves, and only the compression and power stroke are simulated. To account for cyclic symmetry, a periodic boundary condition is applied to the front and back faces of the sector mesh, while a moving wall boundary condition is applied to the piston bowl. For internal combustion simulations, the piston in the TDC position is recommended for meshing because it corresponds to the minimum volume position in the engine cycle. Establishing the mesh at this position ensures that the movement of the mesh is successful throughout the engine cycle. The mesh is then moved to the IVC position, which is the starting point of the simulation. The hexahedral mesh at the TDC was generated using ICEM software. The mesh contains 48478 cells with a minimum quality of 0.5. During the simulation, all meshes were generated using the Fluent CFD software via a dynamic layering approach [7]. The mesh is deformed on the basis of the movement of the piston.

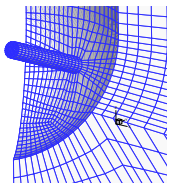

Figure 3. Mesh of the injector hole

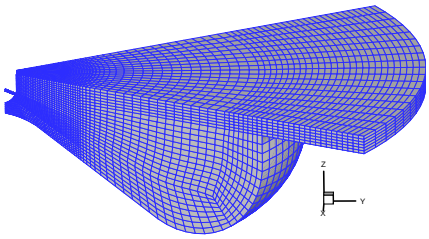

Figure 4. Mesh at the Top Dead Center

The initialization is performed at the IVC position, which corresponds to 147 BTDC.

- The initial pressure and temperature were estimated to be 190000 Pa and 300 K, respectively.
- The swirl ratio is set to 1.5 to initialize the swirl flow field in the combustion chamber using a UDF program provided by Fluent CFD.
- The mass value of the fuel per cycle through the injector hole, the duration of injection, and the form of the injection rate are assigned in a UDF program provided by Fluent CFD.
- The initial air mass and mass of the injected fuel change with the EGR as follows:

$$\text{Initial\_mass\_of\_air\_with\_EGR} = \text{initial\_mass\_of\_air\_without\_EGR} \times (1\text{-}R_{EGR}) \quad (1)$$

$$\text{Fuel\_injected} = (\text{initial\_mass\_of\_air\_with\_EGR})/(\text{air/fuel})_{\text{actual}} \quad (2)$$

- The mass fractions of each species of the oxidizer stream (air + EGR) when EGR is applied are calculated as follows:

$$Y_{(EGR+air)\_intake} = Y_{EGR\_exhaust} \cdot R_{EGR} + Y_{air\_intake} \cdot (1 - R_{EGR}) \quad (3)$$

where $Y_{(EGR+air)\_intake}$ is the mass fraction of each species in the oxidizer stream, $Y_{EGR\_exhaust}$ is the mass fraction of each species in the EGR before its introduction in the oxidizer stream. These mass fractions are calculated from global equations given in the appendix of ref.[8] with excess-air ratio $\varphi_0 = 5$, Y_{air_intake} is the mass fraction of each species in air. The mass values of the fuel injected through the injector hole and the mass fraction of each species in the oxidizer stream for each EGR ratio are given in Tab. 3.

Table 3. Mass of fuel through the injector hole according to the EGR

R_{EGR}	Fuel injected	$Y_{O_2\_intake}$	$Y_{CO_2\_intake}$	$Y_{H_2O\_intake}$	$Y_{N_2\_intake}$
0	11.10×10^{-6}	0.23300	0	0	0.76700
10	09.99×10^{-6}	0.22726	0.00374	0.00306	0.76595
20	8.800×10^{-6}	0.2201	0.00839	0.00687	0.76464
25	8.326×10^{-6}	0.21581	0.01118	0.00915	0.76386
30	7.770×10^{-6}	0.21126	0.01414	0.01157	0.76303

4. Combustion modeling

Non-premixed model and computational sub-models

In this study, turbulent non-premixed combustion is used as a species model with a non-adiabatic energy option. Under the assumption of equal diffusivities, it involves the solution of transport equations for one or two conserved scalars, instead of solving the species equation for each species [9]. This conserved scalar is known as the mixture fraction. The standard k-ε model with standard wall functions is used as the viscous model, and the PISO algorithm is enabled for pressure–velocity coupling. All chemistry calculations are performed using the steady laminar flamelet sub-model, which simulates chemical non-equilibrium in non-premixed combustion [10],[11]. Based on detailed chemical mechanisms, the steady laminar sub-model is used in Fluent CFD to predict the instantaneous relationship between the mixture fraction and thermochemical scalars such as species mass fractions, density, and temperature. These mechanisms are imported into Fluent CFD using a Chemkin file consisting of 22 species and 104 elementary reactions.

Thermal NOx and soot modeling

The thermal formation of NOx is determined by a set of highly temperature-dependent chemical reactions, known as the extended Zeldovich mechanism [12], [13]. To predict soot emissions in Fluent CFD, the Moss–Brookes model is selected because it was primarily developed and validated for methane flames. The Moss–Brookes model describes the evolution of soot through transport equations based on the soot mass fraction and the normalized nuclei concentration. The soot precursor is assumed to be acetylene C_2H_2, which plays a significant role in nucleation and surface growth [14]. The hydroxyl radical OH is assumed to be the dominant oxidizing agent in methane/air diffusion flames [15].

5. Results and Discussion

Velocity profiles

The velocity magnitude contours (case of EGR 0%) at various crank angles are presented in Fig. 5. At the start of injection 9° BTDC, the swirl flow experiences minimal disturbance near the injector hole. Beyond this region, the velocity magnitude remains around 5–10 m/s. As injection proceeds, the fuel jet's momentum progressively induces the flow field. At the TDC, the fuel exits the injector hole at a velocity of 700 m/s, while the flame tip spreads across the bowl surface and reaches the bottom with a velocity of 56m/s, generating a strong vertical flow that facilitates the rapid mixing of fuel and air. The swirl motion is largely dissipated at this crank angle position. It is clear from these results that despite having a higher exit velocity, the methane jet slows down quickly upon penetrating the combustion chamber because of its low density, gaseous state, and faster mixing with air, unlike diesel fuels. A significant amount of methane diffuses from the core to the peripheries of the jet and reacts with O_2 via convective transport. This leads to higher temperatures at the jet periphery of methane. During the late stage of combustion (e.g., 20° ATDC), the jet-induced motion is dissipated, and two vortices are formed, one close to the injector hole and the other above the bowl rim in the squish area. At crank angles corresponding to the downward movement of the piston (e.g., 45° ATDC), the expansion flow dominates, the streamlines are directed downward in the bowl, and the maximum velocity magnitude values are located in the squish and the bowl pit areas.

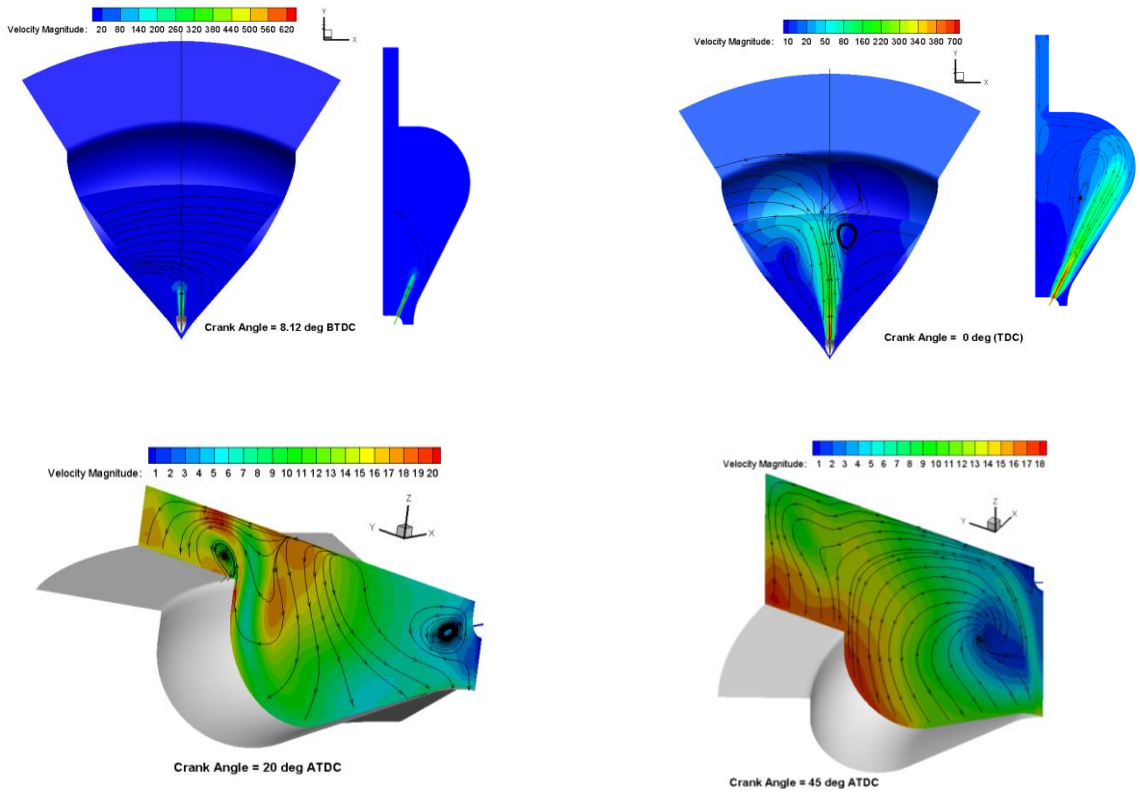

Figure 5. Contours of velocity magnitude at different crankshaft angles

Temperature profiles

Fig. 6 and Fig. 7 illustrate, respectively, the in-cylinder temperature and the O_2 mass fraction contours (case of EGR 0%) at various crankshaft angles. In Fig. 6, the temperature profiles provide a realistic depiction of the combustion process occurring inside the combustion chamber, where the flame emanates from the injector hole. After the start of injection 9°BTDC, the flame surface initially attaches to the bottom of the bowl and then proceeds toward its edge, resulting in an upward direction of the flame. This induces a counterclockwise vortex flow, causing the flame surface to deform and diffuse into a larger area. As a result, a higher combustion temperature is distributed into the upper squish area and the piston bowl pit. Furthermore, due to the swirl effects, the symmetry of the flame around the injection axis is not maintained, which is noticeable at the TDC. The combustion process is shown to be heterogeneous because the temperature is higher and reaches approximately 2500 K in certain regions while remaining significantly lower in others. The temperature variation between these regions decreases as the piston moves down with values ranging from 1000 K to 1700 K. At the TDC position, the combustion process is in progress, resulting in a further rise in the maximum local temperatures, except in the low-temperature zone, where the fuel–air ratio is high due to jet penetration. Around 13°ATDC, as depicted in Fig. 2, the injection process concludes, leading to the cessation of the combustion process. This causes the local temperatures to peak (around 2500 K) in most parts of the flame. The maximum local temperatures stabilize and no longer increase. However, the residual heat produced by the combustion of the remaining injected fuel inside the combustion chamber continues to elevate the overall temperature until approximately 16°ATDC, as indicated by the red line in Fig. 12 (0% EGR case). Fig. 7 illustrates that the distribution of O_2 is inversely consistent with the temperature distribution. More specifically, after the end of the fuel injection at approximately 13°ATDC, regions with higher local temperature values have lower O_2 values and regions with lower local temperature values have higher O_2 values.

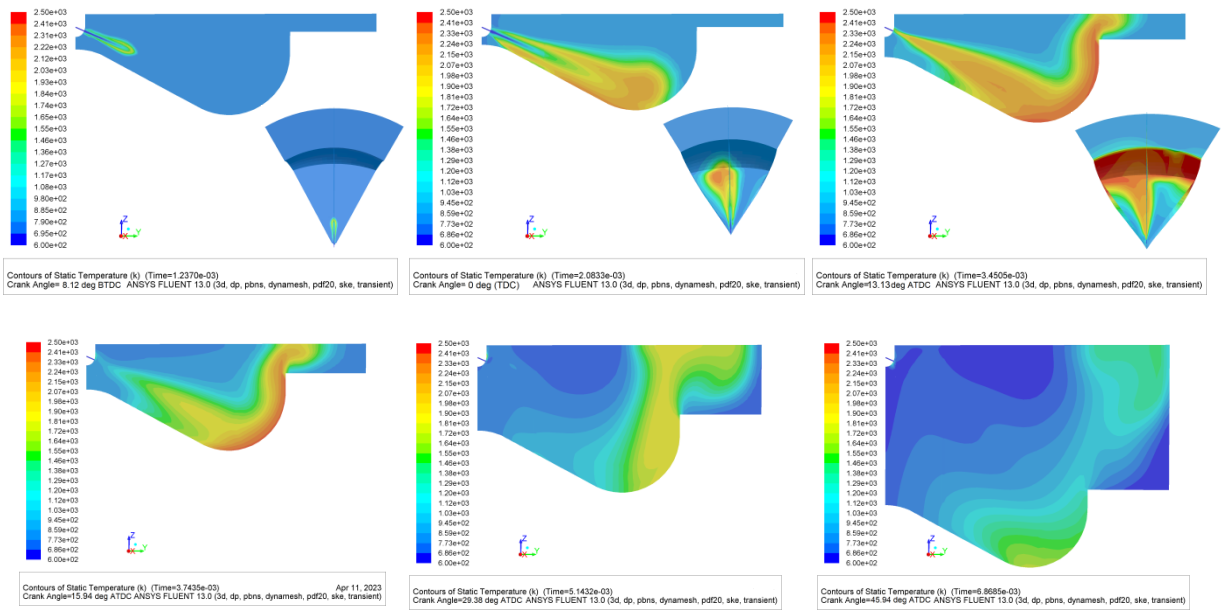

Figure 6. Temperature contours at different crankshaft angles

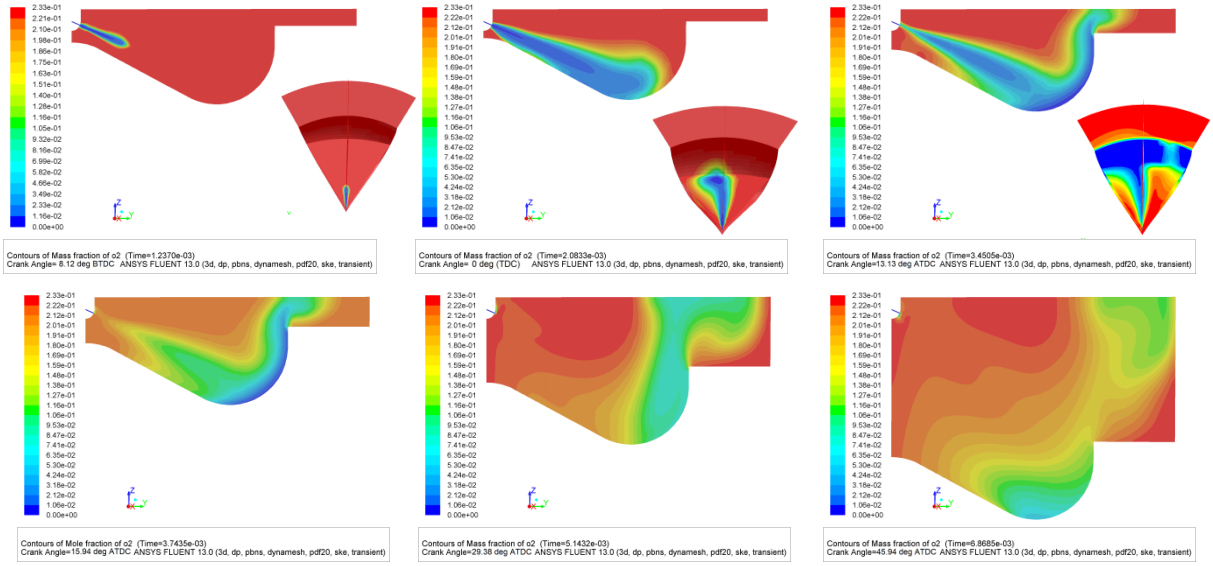

Figure 7. Contours of O_2 mass fractions at different crankshaft angles

NOx emissions

Fig. 8 depicts NOx contours (case of EGR 0%) that demonstrate the relationship between NOx emissions, temperatures, and O_2 in the cylinder, which is explained by the thermal mechanism of NOx formation. In the late phase of combustion, regions exposed to high temperatures and abundant in O_2 exhibit higher NOx levels. According to Fig. 13, NOx becomes visible at approximately 8°ATDC position, which corresponds to the maximum in-cylinder mean pressure, as shown by the red line in Fig. 11. At this stage, a higher temperature zone is located in the piston bowl pit, which is characterized by lower oxygen content, leading to the production of only a small amount of NOx. At approximately 28°ATDC, NOx reaches its peak concentration, as shown by the red line in Fig. 13. These NOx concentrations are located in two adjacent regions, one at the bottom of the bowl and the other around the squish area. Subsequently, in the expansion stage, the maximum local concentration of NOx decreases as the volume increases, while the overall amount of NOx in the cylinder remains constant, as shown in Fig. 13.

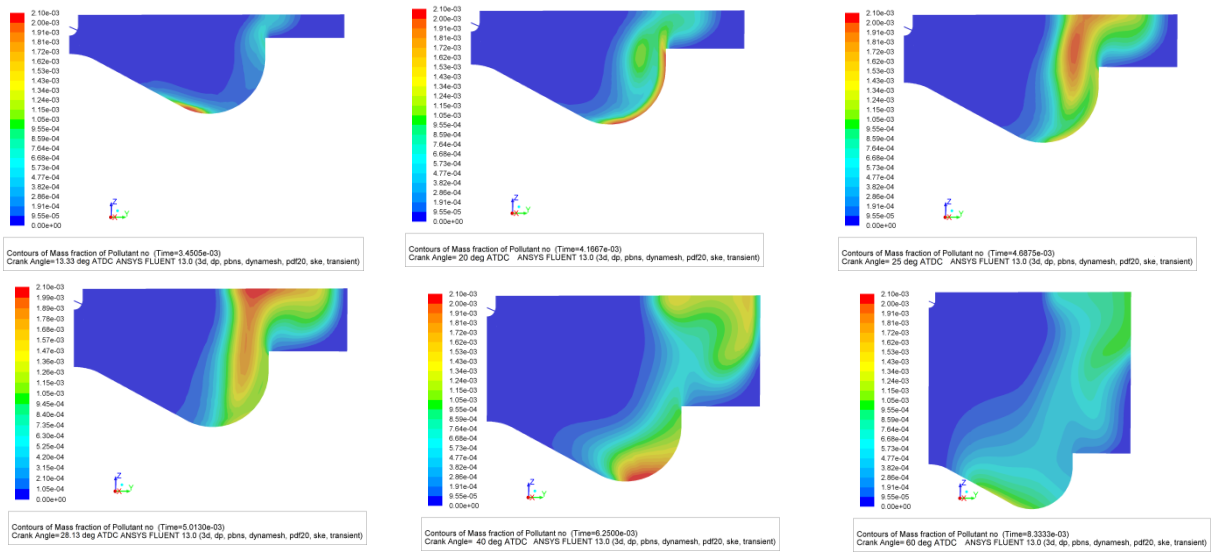

Figure 8. Contours of NOx mass fractions at different crankshaft angles

Soot emissions

Fig. 9 depicts the spatial evolution of the soot mass fractions (case of EGR 0%). The region with higher soot mass fractions is located near the bowl wall and is tilted from the middle plane owing to swirling motion. This observation is further supported by an examination of the velocity and temperature distributions shown in Fig. 5 and Fig. 6, respectively. These soot contours exhibit a temporal trend similar to that of the soot curve (case of EGR 0%), as shown by the red line in Fig. 14–a. Indeed, within the 3-7°ATDC range, a localized area of soot begins to migrate within the bowl pit as the flame gradually expands toward the bowl rim. This migration is accompanied by a rapid increase in the overall soot mass, which peaks at approximately 7° ATDC. The increase in the soot mass fraction can be attributed to the increase in the C_2H_2 mass fraction, as shown in Fig. 10. In the 7–10°ATDC range, a rapid reduction of the soot is observed on the bowl rim and then disappears as the crank angle position exceeds 10° ATDC. Consequently, there is an overall decrease in the soot mass within the cylinder during this period. This decrease can be attributed to C_2H_2 mass fraction, which starts to decline from the same position of 7°ATDC, as depicted in Fig. 10. In the 10–15°ATDC range, soot gradually expands within the bowl pit until approximately 15°ATDC, resulting in an increase in the overall soot mass once again, as shown in Fig. 14-a. This increase in soot can be attributed to the decrease in fuel velocity penetration starting from the 10°ATDC position, as shown in Fig. 2. The reduction in fuel velocity penetration may limit the rate of fuel–air mixing, thereby promoting the accumulation of soot.

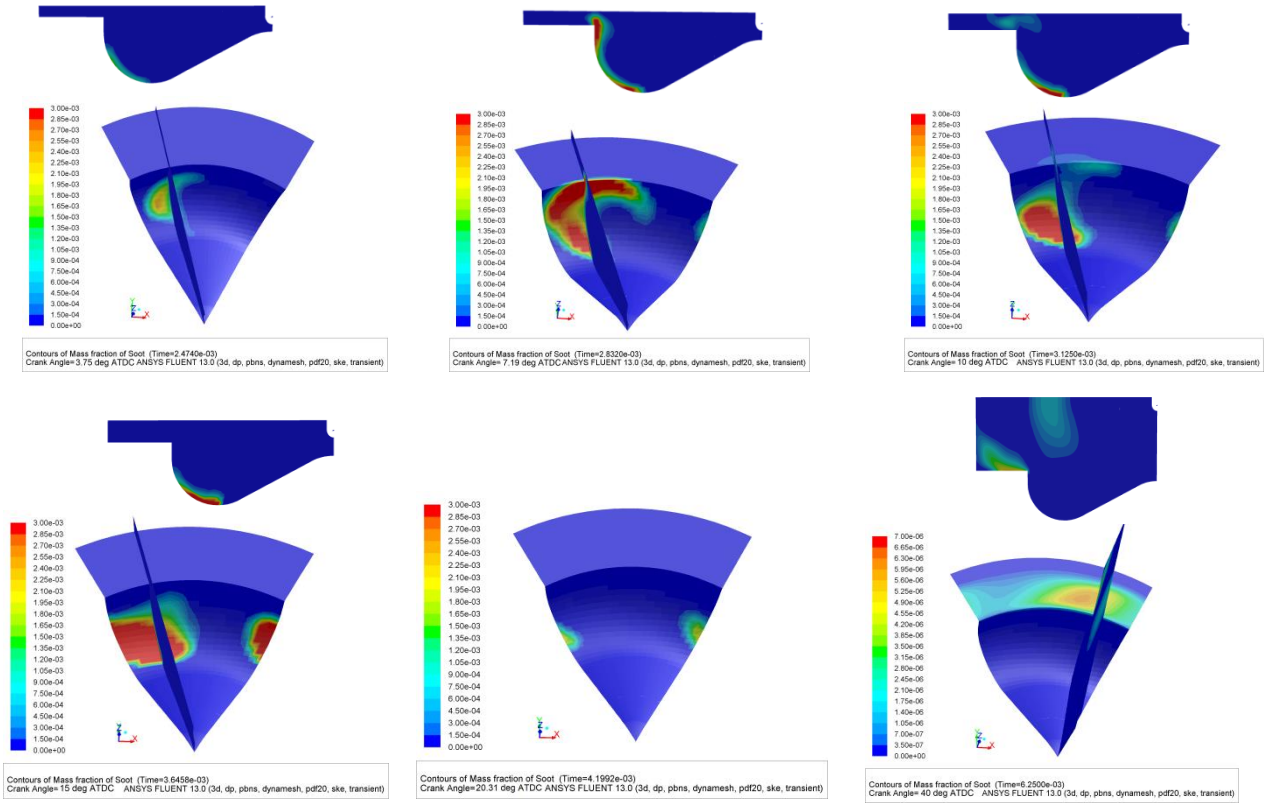

Figure 9. Contours of the soot mass fractions at different crankshaft angles

On the other hand, soot is not observed in the core of the jet where the temperatures are lower. This can be attributed to the fact that high soot levels primarily exist in areas characterized by high temperatures and low oxygen levels, as shown in Fig. 6 and Fig. 7. For instance, a relatively high soot mass fraction of 0.003 is localized within the temperature range of 2350–2450 K. From 15°ATDC position, soot experiences oxidation process simultaneously with the decline of the oxidant OH radicals and rapidly dissipates at approximately 20°ATDC, as shown in Fig. 9 and Fig. 10. From 40°ATDC and during the expansion stage, only areas with low mass fractions of soot remain in the squish and the upper part of the combustion chamber. Furthermore, the level of soot formation is significantly lower than that of NOx, as illustrated in Fig. 8 and Fig. 9. This difference is particularly prominent during the expansion stage, where NOx emissions exceed soot emissions by more than 1000 times. This highlights the potential of natural gas as an effective means of reducing soot emissions, which can be largely attributed to the lower carbon content of natural gas compared with diesel fuels.

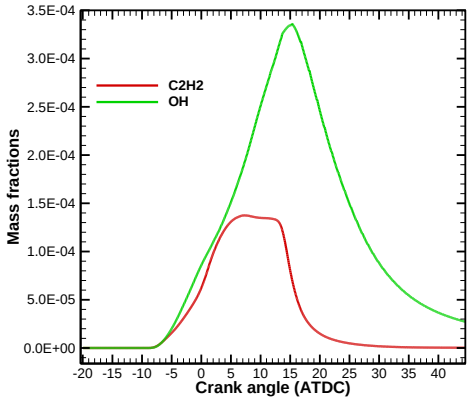

Figure 10. OH and C_2H_2 mass fractions

EGR effect:

In Fig. 11 and Fig. 12, the in-cylinder mean pressure and mean temperature histories are displayed for the five EGR ratios (0, 10, 20, 25, and 30%). As shown in Fig. 11, the peak of the mean pressure experiences a reduction of 0.87 MPa when the EGR ratio is increased from 0% to 30%, resulting in an 8% drop. Correspondingly, the peak of the mean temperature is lowered by 150°C, leading to a 12% decrease. The reason is that when the EGR ratio is higher, the inert components lower the oxygen concentration in the cylinder. This slows down the combustion process and reduces both the peak of pressures and temperatures. Consequently, this leads to lower NOx emissions.

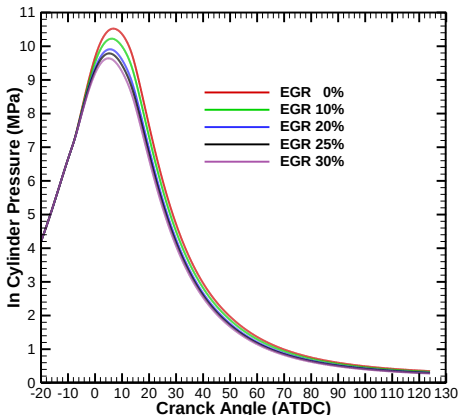

Figure 11. Mean pressure

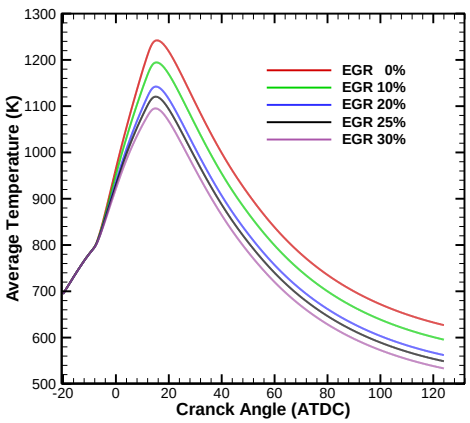

Figure 12. Mean temperature

Fig. 13 illustrates the NOx emission history for the five EGR ratios. For the 0% EGR ratio, the formation of NOx starts at 4°BTDC and is frozen at its peak value at approximately 29°ATDC. As the EGR ratio increases, the initiation of NOx formation is progressively delayed and the rate of increase diminishes. Notably, engine-out NOx emissions exhibit a reduction of 70% when the EGR ratio is increased from 0% to 30%. This indicates the significant impact of EGR on mitigating NOx emissions from the engine. Moreover, the experimental engine-out NOx emissions from diesel fuel [6] are 30% higher than those from natural gas with 0% EGR ratio.

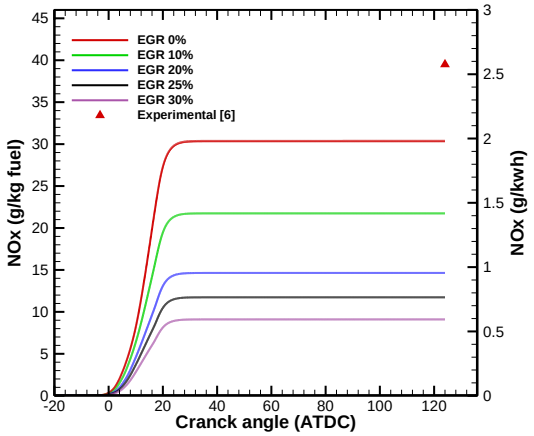

Figure 13. NOx

The amount of soot with respect to the crank angle for the five EGR ratios is presented in Fig. 14-a and Fig. 14-b using both arithmetic and logarithmic scales. These plots provide clear evidence that as the EGR ratio increases, the amount of soot decreases. This finding contradicts the usual expectation that higher EGR ratios would lead to increased soot levels, especially when the amount of injected fuel is kept constant. This decrease in soot is primarily attributed to the decrease in the amount of fuel injected as the EGR ratio increases, despite the reduction in oxygen levels, as indicated in Tab. 3. Moreover, the expanded distribution of the reduced injected fuel over the same injection duration enhances fuel and air mixing, resulting in reduced soot production. Analyzing the plot with an arithmetic scale for 0% EGR, it can be seen that the formation of soot begins at 2°ATDC, and the first peak value is quickly reached at approximately 7°ATDC. As the EGR ratio increases, the initiation of soot formation is progressively delayed, resulting in a gradual shift of the first peak values for each EGR ratio. However, the second peak values consistently occur at the same time for all EGR ratios, precisely at 15°ATDC. Furthermore, these second peak values become gradually lower than the first peak values for high EGR ratios. In addition, it is notable that the soot production rate for a 0% EGR ratio is significantly higher than that for a 30% EGR ratio, resulting in a maximum soot mass approximately four times higher. From the plots with logarithmic scales in Fig. 14-b, it can be observed that after soot production exceeds its maximum value, soot oxidation becomes the dominant process. The main stage of oxidation is characterized by a rapid reduction in soot levels and persists until approximately 22° ATDC. This initial stage is followed by a second stage, during which the soot oxidation rate uniformly slows for all cases of EGR, eventually converging to extremely low values. Comparing the engine-out of soot to its maximum value, it can be observed that approximately 99.64% of the soot mass is oxidized for 0% EGR ratio, whereas approximately 99.97% is oxidized for 30% EGR ratio. In addition, the experimental engine-out soot emissions from diesel fuel [6] are approximately 27 times higher than those from natural gas with 0% EGR ratio.

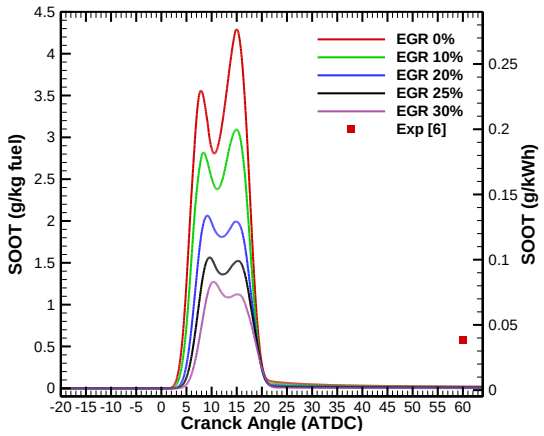

Figure 14-a. Soot (arithmetic scales)

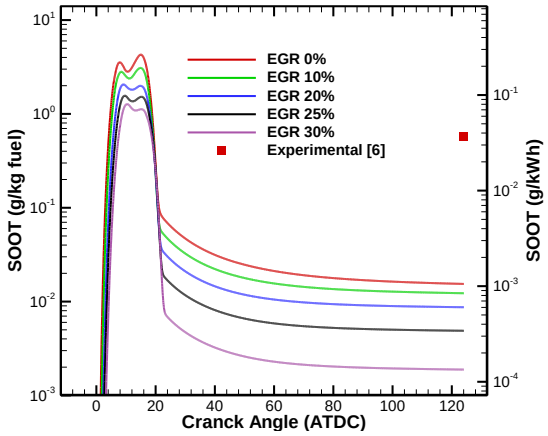

Figure 14-b. Soot (logarithmic scales)

Conclusions

To achieve a trade-off between NOx and soot pollutants, various strategies inside the cylinder can be combined. In this study, two effective approaches were chosen for simulations: using natural gas (methane) as an alternate fuel and employing the EGR technique. The simulations used non-premixed turbulent combustion based on the flamelet approach. To predict pollutant emissions, the Zeldovich mechanism for thermal NOx and the Moss– Brookes model for soot were employed. The study involved varying EGR ratios, specifically 0%, 10%, 20%, 25%, and 30%. The results of these simulations lead to a noteworthy conclusion: applying an EGR ratio of 30% allows for a significant reduction in NOx emissions without an increase in soot emissions. Consequently, this approach enables agreement with authorized standards for heavy-duty engines without significantly compromising their performance. For further studies, it is recommended to extend the simulations to explore various engine parameters. These may include timing injection, mass rate of the injected fuel, rate injection shaping, optimization of combustion chamber shapes, injector diameter, and other relevant variables. By investigating these factors, researchers can gain a more comprehensive understanding of the effects of different engine configurations on emissions and engine performance. This will contribute to ongoing efforts to develop cleaner and more efficient diesel engines that meet stringent emission regulations.

Nomenclature

ATDC – after the top dead center
BTDC – before the top dead center
CA – crank angle
DING – direct injection of natural gas
EGR – exhaust gas recirculation
EVO – exhaust valve open
IVC – intake valve close
R_{EGR} – exhaust gas recirculation ratio
TDC – top dead center
Y_i – mass fraction of species i

Greek symbols
φ_0 – excess-air ratio

Subscripts
i – species number

References

[1] Hodgins BK, Philip GH, Ouellette P, Hung P. "Directly injected natural gas fuelling of diesel engines", SAE Paper No. 961671, 1996.
[2] I.M.Gogolev, J.S.Wallace, "Performance and emissions of a compression-ignition direct-injected natural gas engine with shielded glow plug ignition assist", Energy conversion and management, 164 (2018) pp. 70-82.
[3] Keith Vertin, "Development of a Direct Injected Natural Gas Engine System for Heavy-Duty Vehicles", Final Report, February 2000, Caterpillar, Inc, Peoria, Illinois.
[4] B.Bartunek, U.Hilger, "Direct Induction Natural Gas (DING): A Diesel Derived Combustion System for Low Emissions and High Fuel Economy", 2000, SAE International.
[5] Ladommatos N, Abdelhalim SM, Zhao H, Hu Z. "The effects of carbon dioxide in exhaust gas recirculation on Diesel engine emission", Proc Instn Mech Engng part D J AutomEngng 1998.
[6] A.R. Binesh, et al. "Three-dimensional modeling of mixture formation and combustion in a direct injection heavy-duty diesel engine", Int Journal of Aerospace and Mechanical Engineering, 2008.
[7] ANSYS Inc. Fluent User Guide and Fluent Theory Guide, version 13.0, 2010.
[8] R.Hadjab, M.Kadja, "Computational fluid dynamics simulation of heat transfer performance of exhaust gas re-circulation coolers for heavy-duty diesel engines", Thermal science, 22 (2018) 6B, pp. 2733-2745.
[9] Y. R. Sivathanu and G. M. Faeth. "Generalized State Relationships for Scalar Properties in Non-Premixed Hydrocarbon/Air Flames". Combustion and Flame. 82. (1990) pp. 211–230.
[10] K. N. Bray and N. Peters. "Laminar Flamelets in Turbulent Flames". In P. A. Libby and F. A. Williams, editors Turbulent Reacting Flows. Academic Press. 63–114. 1994.
[11] N. Peters. "Laminar Diffusion Flamelet Models in Non Premixed Combustion". Prog. Energy Combust. Sci. 10. (1984) 3, pp.319–339.
[12] D.l.Baulch et al. "Evaluated kinetic data for high temperature reactions". 1,2,3. Butterworth 1973.
[13] R.K. Hanson and S.Salimian. "Survey of Rate Constants in H/N/O Systems". In W. C. Gardiner, editor Combustion Chemistry. 361. 1984.
[14] S.J. Brookes and J.B.Moss. "Prediction of Soot and Thermal Radiation in Confined Turbulent Jet Diffusion Flames". Combustion and Flame. 116. (1999) 4, pp. 486–503.
[15] C.P.Fenimore and G.W.Jones, "Oxidation of soot by hydroxyl radicals". J. Phys. Chem. 71, (1967) 3, pp. 593–597.
[16] K. Pan, J. Wallace, Computational studies of fuel injection strategies on natural gas combustion characteristics in direct-injection engines, Fuel Volume 288, 2021, 119823.
[17] T. Korakianitis, A. Namasivayam, R. Crookes: Natural-gas fueled spark-ignition (SI) and compressionignition (CI) engine performance and emissions, Prog Energy Combust Sci, 37 (2011) 1, pp. 89 -112.
[18] G. Papageorgakis, A. Agarwal, G. Zhang, D. Assanis: Multi-dimensional modeling of natural gas injection, mixing and glow plug ignition using the kiva-3 code, American Society of Mechanical Engineers, New York, NY (United States), Tech. rep. (1996)
[19] K. Pan, J.S. Wallace: Numerical studies of the ignition characteristics of a high-pressure gas jet in compression-ignition engines with glow plug ignition assist: Part 1-operating condition study, Int. J. of Engine Res., 18 (2017) 10, pp. 1035-1054.
[20] K. Pan, J.S. Wallace: Numerical studies of the ignition characteristics of a high-pressure gas jet in

compression ignition engines with glow plug ignition assist: Part 2-effects of multi-opening glow plug shields, Int. J. of Engine Res., 19 (2018) 9, pp. 977-1001.
[21] K. Pan, J.S. Wallace: Soot and combustion models for direct-injection natural gas engines, Int J Engine Res 23 (2020) 1, pp. 150-166
[22] K. Pan, J.S. Wallace: Soot and combustion models for direct-injection natural gas engines, Int J Engine Res, 23 (2020) 1, pp. 150-166.
[23] K. Pan, J.S. Wallace: A low temperature natural gas reaction mechanism for compression ignition engine application, Combust Flame, 202 (2019) pp 334–346.
[24] B.Yadollahi, M.Boroomand: A numerical investigation of combustion and mixture formation in a compressed natural gas DISI engine with centrally mounted single-hole injector, J Fluids Eng, 135 (2013) 9, 091101.
[25] Ouellette, P., Mtui, P., and Hill, P., "Numerical Simulations of Directly Injected Natural Gas and Pilot Diesel Fuel in a Two-Stroke Compression Ignition Engine," SAE Technical Paper 981400, 1998.
[26] Kurniawan, W.H., Abdullah, S. "Numerical analysis of the combustion process in a four-stroke compressed natural gas engine with direct injection system". J mech sci technol 22, (2008) pp. 1937-1944.
[27] Khatamnezhad Hassan et al. "Incorporation of EGR and split injection for reduction of NOx and soot emissions in DI diesel engines", Thermal Science, 15 (2011) Suppl. 2, S409-S427.
[28] Nemati Arash et al. "Decreasing the emissions of a partially premixed gasoline fueled compression ignition engine by means of injection characteristics and EGR", Thermal Science, 15 (2011) 4, pp. 939-952.
[29] Bencherif Mohamed et al. "Numerical analysis of injection parameters influence on diesel engine performances and emissions correlated by maximum in-cylinder pressure", Thermal Science, 2023.
[30] He Zhixia et al. "A numerical study of the effects of injection rate shape on combustion and emission of diesel engines", Thermal Science, 18 (2014) 1, 67-78.
[31] Zhang Zhi-qiang et al. "A simulated study on the performance of diesel engine with ethanol-diesel blend fuel", Thermal Science, 17 (2013) 1, pp.205-216.
[32] Rafig Babayev et al. "Computational comparison of the conventional diesel and hydrogen direct-injection compression-ignition combustion engines", Fuel, Volume 307, 2022, 121909

Submitted: 27.11.2023.
Revised: 09.05.2024.
Accepted: 14.05.2024.